Chapter 3

MEASUREMENTS OF DRAG REDUCTION AND EXTENSIONAL RHEOLOGY OF DEGRADING POLYMER SOLUTIONS

3.1 Introduction

In transporting fluids between locations (i.e., oil through long pipelines) or cycling fluids within a closed system (i.e., heat transfer fluids in a vehicle), substantial energy expenditure comes from pumping the fluid to overcome the friction (drag) experienced during turbulent flow. One method currently employed industrially to reduce that friction (such as in the Trans-Alaska pipeline)[1] is polymeric drag reduction, where a high molecular weight polymer additive in a fluid results in increased flow rates at the same pressure differential. Applications of polymeric drag reduction, however, are limited by mechanical chain scission of polymer backbones, which causes a decrease in the molecular weight of the polymer additive and thus a decrease in efficacy over time, particularly in high flow rate elements of flow, such as pumping (see Chapter 2 for further discussion of chain scission).[2–7] The Kornfield group has sought to develop end-associative polymeric additives to be scission-resistant (see Chapter 1 for discussion of megasupramolecules)—these megasupramolecular polymer systems have previously demonstrated drag reduction without degradation in fuel.[8] To intentionally design additives for new applications and fluids, such as water instead of fuel, we need to understand the underlying mechanisms of polymeric drag reduction; however, polymeric drag reduction couples two complex problems: polymer conformations under flow and turbulence.

History and Features of Polymeric Drag Reduction

The phenomenon of drag reduction was independently discovered by multiple individuals during World War II, including B.A. Toms and Karol Mysels, and published in the years following.[9–12] In the case of Toms, the study of drag reduction was a byproduct of trying to understand why polymer additives for lubricants were degrading under flow—characterizing degradation and chain scission has been a part of the drag reduction field since its inception.[11,12] Historically, the mechanism of turbulent polymeric drag reduction has been debated extensively, with most theories only fitting a subset of empirical observations.[13,14] Key features of polymeric drag reduction that theory seeks to explain include the onset, the velocity profile near the wall, the maximum drag reduction asymptote, and, more recently of interest, intermediate regimes of drag reduction. The onset of polymeric drag reduction is both a function of the flow conditions and the solution properties, and is typically experimentally characterized by the Reynolds number (either bulk Reynolds—$Re = \rho UD/\eta_{shear}$, where ρ is the density, U is the mean velocity, D is the length scale of the flow, and η_{shear} is the shear viscosity—or the friction Reynolds number—$Re_\tau = D\sqrt{\tau_w}/\eta_{shear}\sqrt{\rho}$, where τ_w is the wall shear stress) and the combination of concentration, polymer molecular weight, and backbone identity. In simulation work, those polymer properties relative to the fluid flow are bundled into the Weissenburg number ($Wi = \lambda\dot{\epsilon}$, where λ is the relaxation time of the polymer and $\dot{\epsilon}$ is the rate of strain on the polymer).[14] The near-wall mean velocity profile in the log-law region, as initially captured by Virk and coworkers, is seen in polymeric solutions in turbulent flow to transition from the Newtonian case (the Prandtl-Kármán law) to a maximum drag profile with increasing drag reduction.[15–19] That maximum drag profile is one reported characteristic of the maximum drag regime (MDR, also called the

maximum drag asymptote), a regime that appeared universal in which further raising the Reynolds number, the polymer molecular weight, or the concentration of polymer would not further increase the measured drag reduction.[17,18,20] Research after Virk has characterized two additional intermediate regimes of drag reduction—a low-extent drag reduction regime (LDR) and a high-extent drag reduction regime (HDR)—that have distinct mean velocity profiles and fluctuation characteristics, with an empirical transition around a percent drag reduction of 30-35 %.[14,21]

Experimentally, bulk measurements of drag reduction have been used since the 1940s to determine how much polymer additives can reduce friction. In last 25 years, particle image velocimetry (PIV), a technique in which particles sufficiently small to not disrupt the flow (but sufficiently large to track) are added to the fluid of interest and then observed using a high-speed camera, has become a powerful technique for looking at the microscale effects on turbulent structures correrspondingto bulk effects.[22,23] Degradation of polymers has limited the ability to use both macro and micro techniques to their full extent reproducibly. For example, in PIV, observations of turbulent flow may be assumed to be at quasi-steady state, to be able to average over a series of measurements to obtain a mean velocity profile. If the polymer is degrading within the viewing window, a mean velocity profile obtained via averaging becomes less meaningful. On the other hand, simulation has opened a window into the interaction of polymers with turbulent flow structures, uncovering details that would be smaller than the observable scale in experiments and without necessarily being constrained by degradation. Due to limited processing power, however, simulation cannot yet reach high Reynolds numbers ($Re_\tau > 100 - 1000$) for sufficiently large domain sizes and long times with practical amounts of computing resources.[14]

The community studying drag reduction, as a result, is pushing the limits of these techniques to find opportunities for overlap between experiment and simulation, fill gaps in our collective knowledge, and evaluate potential theories. Recent simulation work has iterated through a number of hypotheses,[1,14,20,24] challenging our conceptions of the nature of drag reduction and its long established regimes. In relatively small simulation box sizes, turbulent drag reduction was observed to consist over time of bursts of active Newtonian turbulence followed by "hibernation," where the behavior mimicked that of MDR. By varying Wi, modulation between these two extremes was achieved.[1,25] Extension of these simulation techniques to larger box sizes revealed that what was appeared to be purely temporal on a small scale was instead a spatio-temporal phenomenon, in which hibernation was observed to only affect subdomains of flow, rather than the entire domain simultaneously.[20,26]

A relatively recent discovery in polymeric drag reduction is the regime of elasto-inertial turbulence (EIT). EIT can occur at lower Reynolds numbers than Newtonian turbulence, but sufficiently high Re that inertia cannot be neglected (unlike in elastic turbulence). In the presence of the elasticity from a polymer additive, EIT suppresses Newtonian turbulence and approaches the maximum drag asymptote as Re increases.[24] In addition to introduction of EIT as a potential mechanism for polymeric drag reduction, work examining MDR has also found that the behavior is not as universal as originally thought, exhibiting hibernation and relaminarization behavior at Reynolds numbers near the transition between laminar and turbulent flow, while demonstrating characteristics of EIT farther from transition.[19,20,26]

Scope

Because our primary applications of interest for megasupramolecular polymer additives are industrial scale, relevant Reynolds numbers are much higher than what is readily accessible in current simulation work. The scope of this chapter is to describe the design, construction, and characterization of a instrument for simultaneous measurement of polymeric drag reduction in sufficiently high Reynolds number pipe flow via particle image velocimetry and bulk flow rates. We monitored the degradation of an example polymer solution in different elements of the instrument and due to specific actions in our procedure. We acquired preliminary measurements of drag reduction as degradation occurred for two water-soluble polymer backbones, poly(ethylene oxide) (PEO) and polyacrylamide (PAM), while probing the extensional relaxation time of the initial and degraded solutions as a measure of how much chain scission had occurred. In the thesis work of Jacqueline Tawney, validation of particle image velocimetry and measurements of polymeric drag reduction with this instrument are planned, along with use of the measured velocity profile in resolvent analysis, a technique in which the Navier-Stokes equation can be broken down into forcing and response modes,[27,28] allowing insight into the underlying perturbation of turbulence by polymers.

This work describes an ongoing collaboration between members of the groups of Professor Julia Kornfield and Professor Beverley McKeon—detailed descriptions of contributions are documented in the Experimental Section.

3.2 Experimental Section

Materials

Polyethylene oxide acquired from Dow (Polyox WSR301). Polyacrylamide (PAM) was prepared by Hojin Kim. PAM synthetic details to be included in

Table 3.1: Molecular weights, dispersities, and sources for polyacrylamide (PAM) and poly(ethylene oxide) (PEO) samples.

Backbone	M_w (Mg/mol)	M_n (Mg/mol)	Đ	Sample Name	Source
PAM	6.70	5.00	1.3	6.7M PAM	HK
PEO	6.00	3.80	1.6	6M PEO	Dow WSR301

M_w: Weight-average molecular weight, M_n: Number-average molecular weight,
Đ: Dispersity index (M_w/M_n),
PAM: Polyacrylamide, PEO: Poly(ethylene oxide),
HK: Hojin Kim

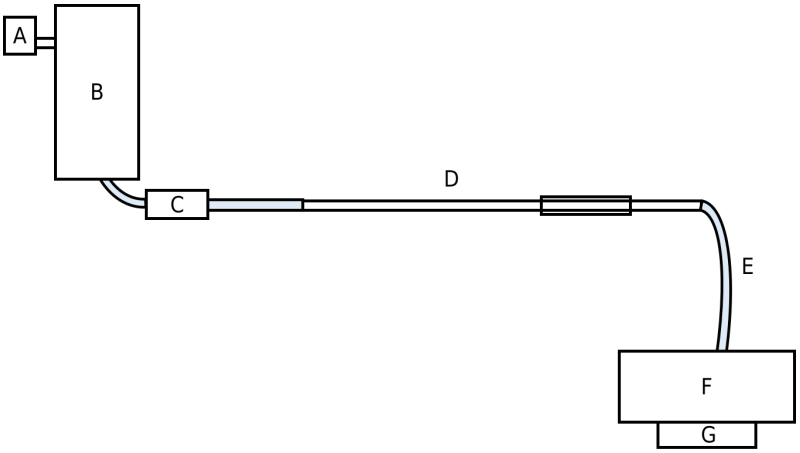

Figure 3.1: Schematic of drag reduction instrument.

the thesis of Hojin Kim. Table 3.1 includes number-average molecular weight (M_n), weight-average molecular weight (M_w), dispersity (Đ), and source for polymers used in this chapter.

Drag Reduction Instrument Construction

The instrument used in the drag reduction measurements described below was designed, constructed, and refined in collaboration with Dr. David Huynh, Dr. Ryan McMullen, and Jacqueline Tawney, members of Professor Beverley McKeon's group. Without the collaboration with Professor McKeon and her students, these experiments would not have been possible.

The drag reduction instrument consists of a reservoir tank (**B**, Figure 3.1)

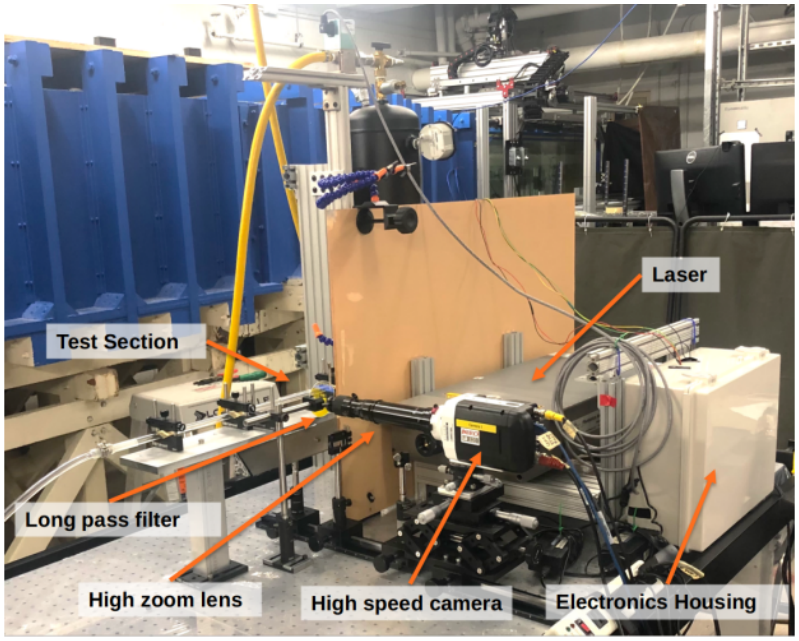

Figure 3.2: Photo of drag reduction instrument with optical components labeled. Image provided by Jacqueline Tawney, used with permission.

that can be pressurized using a pressure regulator (**A**, ProportionAir QB3), a ball-valve (**C**, DynaQuip 1AWH8) connected to the reservoir tank and to the quartz optical section (**D**) by flexible polytetrafluoroethylene tubing (**E**), and a receiving tank (**F**) on a scale (**G**) also connected to the quartz optical section by flexible tubing. The flexible tubing between the quartz optical section and the receiving tank can be exchanged to change the length of the total tube length for determination of the pressure differential not including the head leosses at the inlet and outlet. The two total lengths were 4.27 m ("short") and 5.89 m ("long"). For contraction experiments, the receiving tank is connected directly to the ball valve via a 16 cm segment of flexible tubing. The instrument was assembled by Dr. David Huynh and Dr. Ryan McMullen and adapted and validadated by Jacqueline Tawney.

The optical section of the instrument (test section in 3.2) is a long cylindrical quartz tube with a small section of square tubing with a cylindrical center

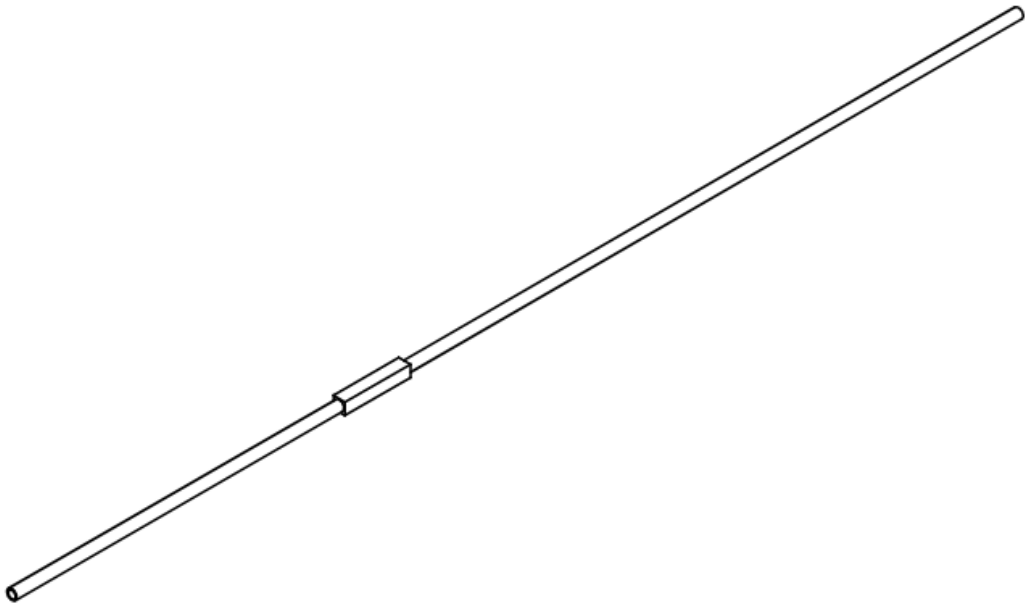

Figure 3.3: Isometric view of quartz optical section with cylindrical section for flow and rectangular segement for optical viewing

inserted into the center (Figure 3.3). I designed the final optical section in collaboration with Dr. David Huynh and Dr. Ryan McMullen, and the piece was constructed by PGB Optical, based on initial prototypes I built using commercially available quartz sections and optical glue.

To make repeated experiments practical and reproducible, I designed and installed a custom Arduino-operated system for operating the ball-valve and pressure regulator and for measuring the pressure at the regulator and the reservoir tank and the mass at the receiving tank. Jacqueline Tawney and I refined and rebuilt the custom system to be more robust. Jacqueline Tawney then enclosed all possible electrical components in a water-resistent enclosure for safety.

I programmed a LabVIEW graphical user interface to simultaneously record the mass measurements and issue commands to the Arduino-operated system to control each part of the instrument. The recorded mass measurements are

automatically saved to text files. Jacqueline Tawney then performed analysis in MATLAB to extract the steady-state mass flow rate for each experiment.

Particle image velocimetry measurements using this instrument are planned to be part of the thesis of Jacqueline Tawney.

Solution Preparation

As discussed above, long polymer chains are vulnerable to mechanical degradation. We sought to minimize degradation prior to running samples in the instrument.

Stock solutions of polymer in deionized water were prepared by adding solid polymer to a 2L glass vessel of deionized water with a stir bar creating a vortex to distribute the solid polymer throughout the volume of water and reduce clumping. After polymer was fully added, stirring was stopped to prevent high shear conditions at the bottom of the vessel. The glass vessel was placed on a roller at 30 rpm for 7-10 days at ambient temperature, 15 $\pm$ 1 °C. During rolling, the vessels were covered in aluminum foil to reduce chemical degradation of PEO due to light and ultraviolet radiation.

In the case of the PEO solutions, stock solutions were visually homogeneous before use. In the case of PAM stock solution, the initial stock solution had small flakes of undissolved polymer after over a week of rolling time. After the further dilution described below, polymer clumps were no longer observed.

Stock solutions were diluted to 0.0066 wt% (66 parts-per-million by weight) with deionized water in an opaque drum and rolled for 5 hours at 21 rpm. After rolling, diluted solutions were checked for visual inhomogeneities, and none were observed.

Solutions were used within two weeks of initial stock preparation.

Stock solutions were prepared by Red Lhota. Dilutions to concentrations used in the instrument were completed by Jacqueline Tawney.

The as-prepared 0.0066 wt % solutions were each split into two portions. In case of contraction measurement, one portion of a 6M PEO solution was used for the lower pressure experiment (15 psi, 0.10 MPa) and one portion was used for the higher pressure experiment (20 psi, 0.14 MPa). In the case of drag reduction experiments, one portion each of a 6M PEO solution and a 6.7M PAM solution were used for their own short-tube experiment, and one each was used for their own long-tube experiment. The two PEO solutions were each split into two 7.5 L portions; due to limited polymer availability, PAM solution was split into 4.43 L portions.

Degradation and Drag Reduction Measurements

The following procedures were performed by Jacqueline Tawney. Two related sets of experiments were performed, in addition to two additional samplings (loading and pushback, as discussed below). The first used only the reservoir tank, the ball-valve, a 16 cm segment of flexible tubing, and the receiving tank to measure the degradation as a function of pass due to the contraction from the reservoir tank into the ball valve and the expansion into the receiving tank (referred to below as a contraction experiment). The second used the complete system as described above with Figure 3.1 and measured the degradation and drag reduction as a function of pass from flow from the reservoir tank to the receiving tank.

After mixing and splitting the solutions as described above, a solution portion was loaded into an carboy. An initial sample of the solution added to the carboy was collected. The carboy was attached to the reservoir tank (**B** in Figure 3.1) by a quick-disconnect connector, while the reservoir tank was unpressur-

ized and open to the air, and the ball valve was closed. Fluid was allowed to run from the carboy into the tank through gravity-driven flow through the connection until all of the fluid was in the reservoir tank. In the loading sampling, an additional sample was collected by simulating gravity-driven flow through the quick-disconnect connector from the carboy into a sampling vessel.

After loading the initial fluid, a "pass" would proceed as follows. In a drag reduction, the reservoir tank would be pressurized to 5 psi (0.03 MPa) and the tube connecting the reservoir tank to the receiving tank (**F** in Figure 3.1) would be "primed" with a small amount of solution by opening the ball valve for 2.5 seconds to reduce vibration of the receiving tank from air blowing through prior to solution flow. In a contraction experiment, no priming step was used due to the shorter distance and lack of measurement of the receiving tank's mass. The reservoir tank would be pressurized to the trial pressure. After pressurization, the ball valve would be opened, and solution would flow into the receiving tank. In the case of the contraction experiments, all fluid was allowed to flow into the receiving tank before the ball valve was closed, and the total time of flow and the total mass of fluid remaining in the tank were used to estimate the mass flow rate. In the case of the drag reduction experiments, the mass of the receiving tank was measured as a function of time by the scale (**G** in Figure 3.1) and the ball valve was closed after a set duration (7.5 s for PEO short tests and 7 s for PEO long and all PAM tests). For the measurements of the 6M PEO solution in drag reduction, a second trial was performed by opening the valve again and measuring flow rate a second time at the same pressure. If any additional solution remained in the reservoir tank, it was pushed through at the testing pressure into the receiving tank. The reservoir tank would then be depressurized slowly back to atmospheric pressure.

After passes 1, 5, and 10, the fluid in the receiving tank was sampled. Then, to return the fluid back to the reservoir tank, the receiving tank was pressurized to 5 psi (0.03 MPa) and the ball valve opened ("pushback"). In the pushback sampling experiment, a small portion of the fluid returned to the reservoir tank after pass 1 of a contraction experiment was allowed to flow back into the receiving tank to be sampled.

The above "pass" and "pushback" procedure was repeated for 10 passes. When exceeding 10 passes, the solutions demonstrated too low of relaxation times to be reliably measured in DoSER (discussed in Chapter 1). The solution was then removed from the instrument and disposed of. The instrument was rinsed by loading ∼8 L of deionized water and then allowing flow at 10 psi (0.07 MPa) followed by drying using air at 5-20 psi (0.03-0.14 MPa).

The pressure for the contraction experiments was chosen to mimic the range of flow rates previously achieved in prior drag reduction measurements in the instrument. At 15 psi (0.10 MPa), the mass flow rate was approximately 0.44 kg/s. At 20 psi (0.13 MPa), the mass flow rate was approximately 0.50 kg/s. To extract a measurement of the friction per unit length of tube, the pressure difference required to acheive similar flow rates through a 4.27 m ("short") and 5.89 m ("long") tube for the PEO at 0.0066 wt % on its first pass was determined by Jacqueline Tawney. At 40 psi for the short-tube and 43 psi for the-long tube experiments, the mass flow rates were approximately 0.52 kg/s and 0.50 kg/s respectively. Based on these results, the appropriate pressure difference for wall shear stress calculation was estimated to be 4 psi, which yields a Reynolds number based on the wall shear stress (Re_τ) of $1.8 * 10^3$. The 40 psi for short and 43 psi for long pressures were maintained for the 6.7M PAM solution for consistency.

Dripping-onto-Substrate Extensional Rheometry (DoSER)

A dripping-onto-substrate extensional rheometry (DoSER) instrument was constructed by Robert Learsch and Red Lhota consisting of a GSVitec MultiLED G8 with QT lamp head (12000 lumen light source, Figure 1.7**A**), a Harvard Elite 11 syringe pump on an adjustable track (solution delivery, **B**), Photron FASTCAM Nova S12 type 1000K-M-32GB (high-speed camera, **C**) equipped with an optical train as described below, and a custom holder for aluminum substrates (**D**). The optical train consisted of a Resolve4K 7:1 Zoom Video microscope lens, two rear projection lenses, a 1.0x objective lens, and a coupler, resulting in a resolution limit at full zoom of 3.5 µm (**E**). The camera was operated at 25,000 frames per second with a shutter speed of 150,000 Hz (i.e., 7 µs exposure). The light passes through a diffuser before reaching the measurement plane (**F**).

A syringe with a 22G blunt-tip stainless-steel needle (outer diameter 0.718 mm) was mounted to the syringe pump. The substrate was positioned at a height of 2.8 mm below the tip of the needle, corresponding to a height-to-needle-diameter ratio of 4 or a height-to-initial-droplet-diameter ratio of 1, which is within the optimal range for water solutions.[29] Ambient temperature was measured with each experiment and was in the range 15 ± 1 °C.

For each solution, DoSER was performed using the following procedure. An aliquot was slowly loaded into a syringe through a 22G stainless-steel blunt-tip needle. The syringe was attached to the syringe pump and the syringe pump was slowly advanced until solution was observed to drip from the needle, and then the needle tip was cleaned. A clean set of aluminum substrates was loaded onto the substrate holder and the first substrate was aligned below the needle tip. The light was turned on and the camera was focused and aligned with the needle tip. The substrate was then raised or lowered to the correct

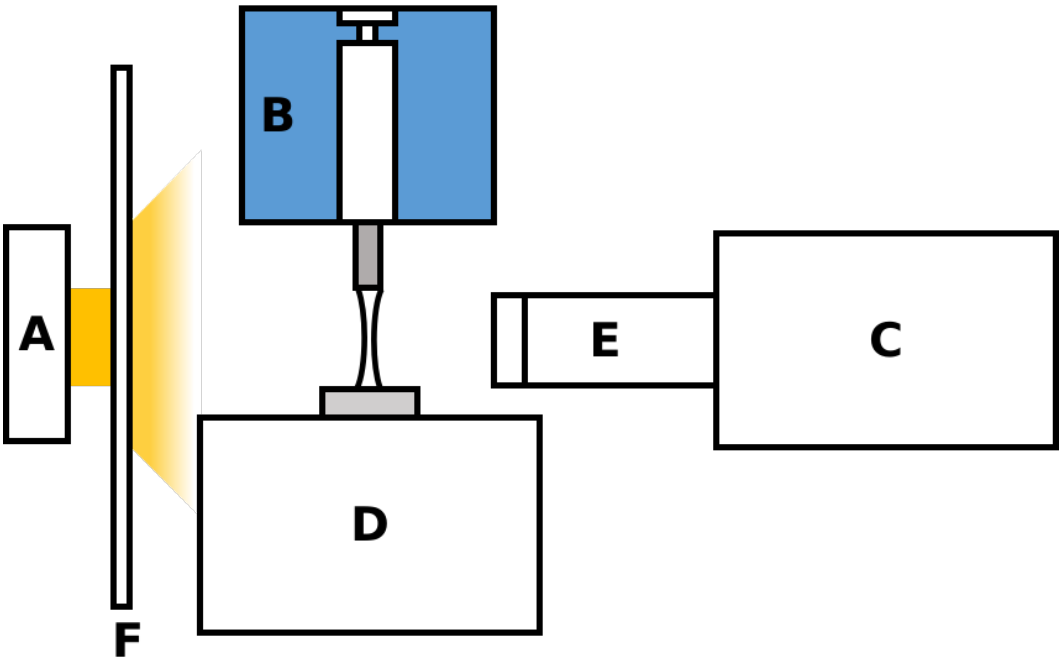

Figure 1.7: Schematic of dripping-onto-substrate extensional rheometer (not to scale). (repeated from page 14)

height (as describe above) relative to the needle tip. A background video with a droplet-free needle and substrate was acquired. A drop was dispensed from the needle tip by the syringe pump at a rate of 0.02 mL/min, until the drop was nearly touching the substrate. The syringe pump was stopped prior to droplet-substrate contact. The events of droplet contact through liquid bridge formation and pinchoff were recorded (referred to as an experimental video or "run"). A clean substrate was then placed below the needle tip. Dispensing drops onto a clean substrate was repeated until five total runs were recorded. The videos were analyzed using the *dosertools* Python package, described in detail in Appendix A, to obtain the normalized diameter as function of time after the critical time (time of transition between solvent behavior and elasto-capillary response). The decay of the normalized diameter is used to evaluate the extensional relaxation time. In our experiments, run-to-run variation on the DoSER instrument was observed to be more significant than errors in

fitting–errors in measured relaxation times are thus quantified using the run-to-run variation. Solutions with relaxation times of 0.05 ms and lower were difficult to consistently characterize on our instrument.

Further discussions of DoSER theory and analysis are available in Chapter 1 and Appendix A respectively.

3.3 Results

Instrument Characterization

To characterize at what point in the solution's time in the instrument the degradation was occurring, we used dripping-onto-substrate extensional rheometry (DoSER) to measure the extensional relaxation time of samples before and after the loading, pushback, and tank-to-ball valve stages of the procedure. To determine extensional relaxation times, we first measured normalized diameter (D/D_0) by image analysis of high-speed videos of DoSER experiments as described in Appendix A, then fits to the normalized diameter in the elastocapillary regime as described in Appendix A were used to determine the extensional relaxation time (λ_E).

Loading the sample into the tank from the carboy resulted in a slight, but not statistically significant increase in the measured extensional relaxation time (Figure 3.4(a)). Pushback at low pressure from the destination tank back to the reservoir tank does not statistically signficantly change the measured extensional relxation time (Figure 3.4(b)).

To determine where degradation primarily occurs in the instrument, Jacqueline Tawney isolated the contraction from the reservoir tank into the ball valve and expansion back into the destination tank for collection (with minimal institial flexible tubing, 16 cm) and flowed a solution of 6M PEO at 0.0066 wt % in deionized water through the system at 15 and 20 psi (0.10 and 0.14

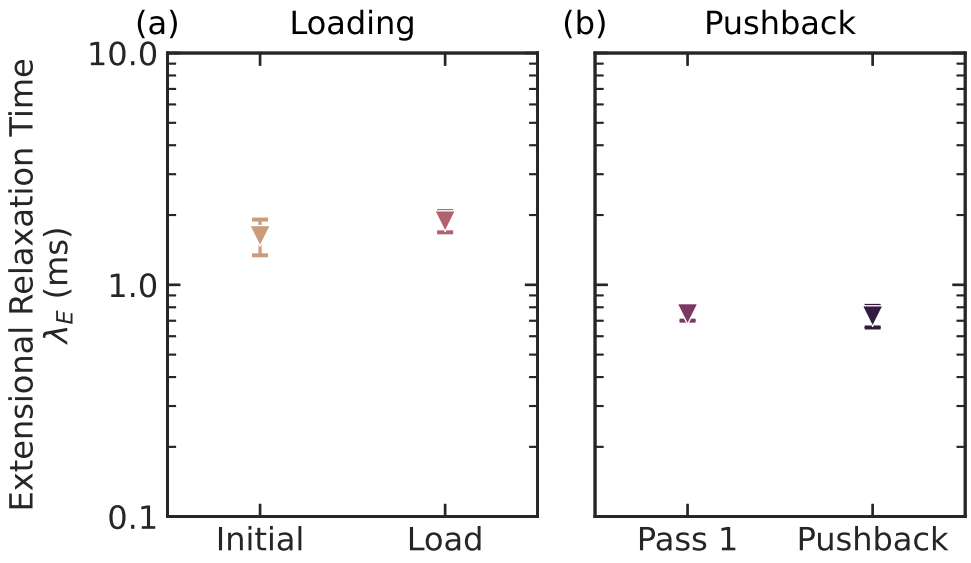

Figure 3.4: Extensional relaxation time (λ_E, ms) of 6M PEO at 0.0066 wt % in water (a) before and after loading from the carboy into the reservoir tank and (b) after a single pass at 15 psi (0.10 MPa) and after pushback from the receiving tank into the reservoir tank. Vertical error bars represent 95% confidence intervals. Where error bars are not visible, the corresponding interval is within symbol size.

MPa, respectively). The fluid achieved flow rates of approximately 0.43 kg/s at 15 psi and 0.50 kg/s at 20 psi, bounding typical flow rates for polymer solutions through the full drag reduction instrument. Aliquots of the initial solution, and of the fluid in the receiving tank after passes 1, 5, and 10, were collected and measured using DoSER (Figure 3.5(a)). Effective molecular weights were calculated from the measured extensional relaxation times as described in Chapter 2 using Equation 2.3 (Figure 3.5(b)). The flow through the contraction resulted in substantially decreased extensional relaxation time and thus effective molecular weight with repeated passes.

Turbulent Drag Reduction

Mass flow measurements were performed for solutions of both 6M PEO and 6.7M PAM at 0.0066 wt % in deionized water for both the short and long

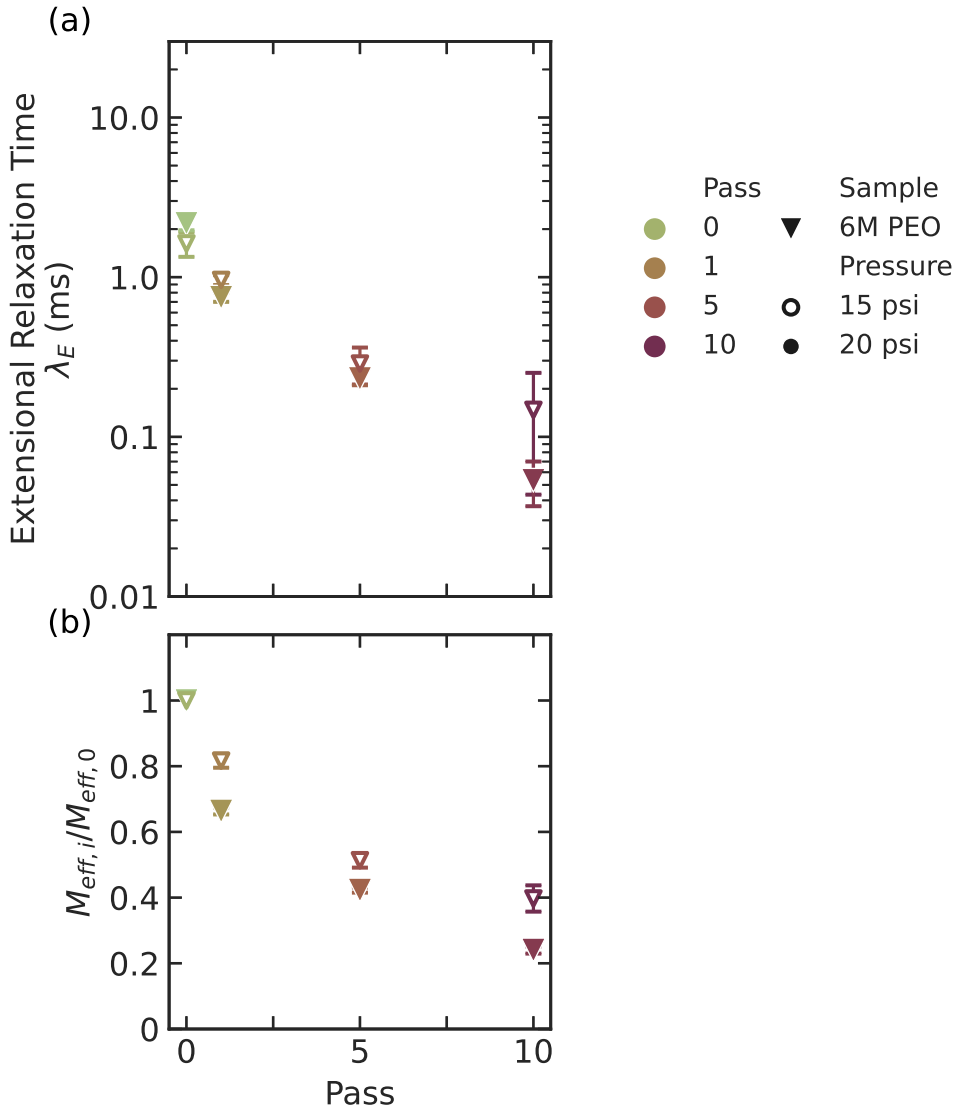

Figure 3.5: Changes with passes through the contraction-expansion of the drag reduction instrument for solutions with as-prepared molecular weight and backbone of 6M PEO at concentrations of 0.0066 wt %. (a) Extensional relaxation time (λ_E, ms) as a function of passes. (b) Ratio of effective molecular weight of degraded samples to initial effective molecular weight as a function of pass ($M_{eff,i}/M_{eff,0}$), given observed extensional relaxation time from (a) using Equation 2.3, assuming a constant total concentration of the solution. Vertical error bars represent 95% confidence intervals representing run-to-run variation in DoSER measurements (fitting errors are substantially smaller). Where error bars are not visible, the corresponding interval is within symbol size.

tubes. These measurements were used to calculate bulk Reynolds numbers for the flow (Figure 3.6(a)). Using a water flow rate at 40 psi through the short tube as our baseline (dashed lines in Figure 3.6(a), $\dot{m}_{water}$), the percent drag reduction (% DR) due to the polymer at each pass was defined using Equation 3.1, where $\dot{m}_{solution,i}$ is the mass flow measured for the solution after pass i (Figure 3.6(b)).

$$\% \ DR_i = \frac{\dot{m}_{solution,i} - \dot{m}_{water}}{\dot{m}_{water}} \tag{3.1}$$

Aliquots of the initial solution, and of the fluid in the reservoir tank after passes 1, 5, and 10, were collected and measured using DoSER (Figure 3.7(a)). Effective molecular weights were calculated from the measured extensional relaxation times as described in Chapter 2 using Equation 2.3 (Figure 3.7(b)).

Using the effective molecular weight ratios calculated from the extension relaxation times measured and multiplying by the known starting molecular weight, we compared the measured drag reduction to the effective molecular weight as the solutions decay. The PEO solutions are at a reduced concentration (weight concentration divided by overlap concentration, c/c^*) of 0.12; the PAM solutions are at c/c^* of 0.05.

3.4 Discussion

Drag Reduction Instrument Design

We considered a number of key features and constraints in the design of the instrument. On the fluid flow side, we sought to reach high Reynolds numbers in pipe flow that were largely unstudied in the literature at the intersection of polymeric drag reduction and particle image velocimetry (PIV), particularly those not reachable by current drag reduction simulation capabilities. Increasing Reynolds number, though, requires high pressures and large volumes of

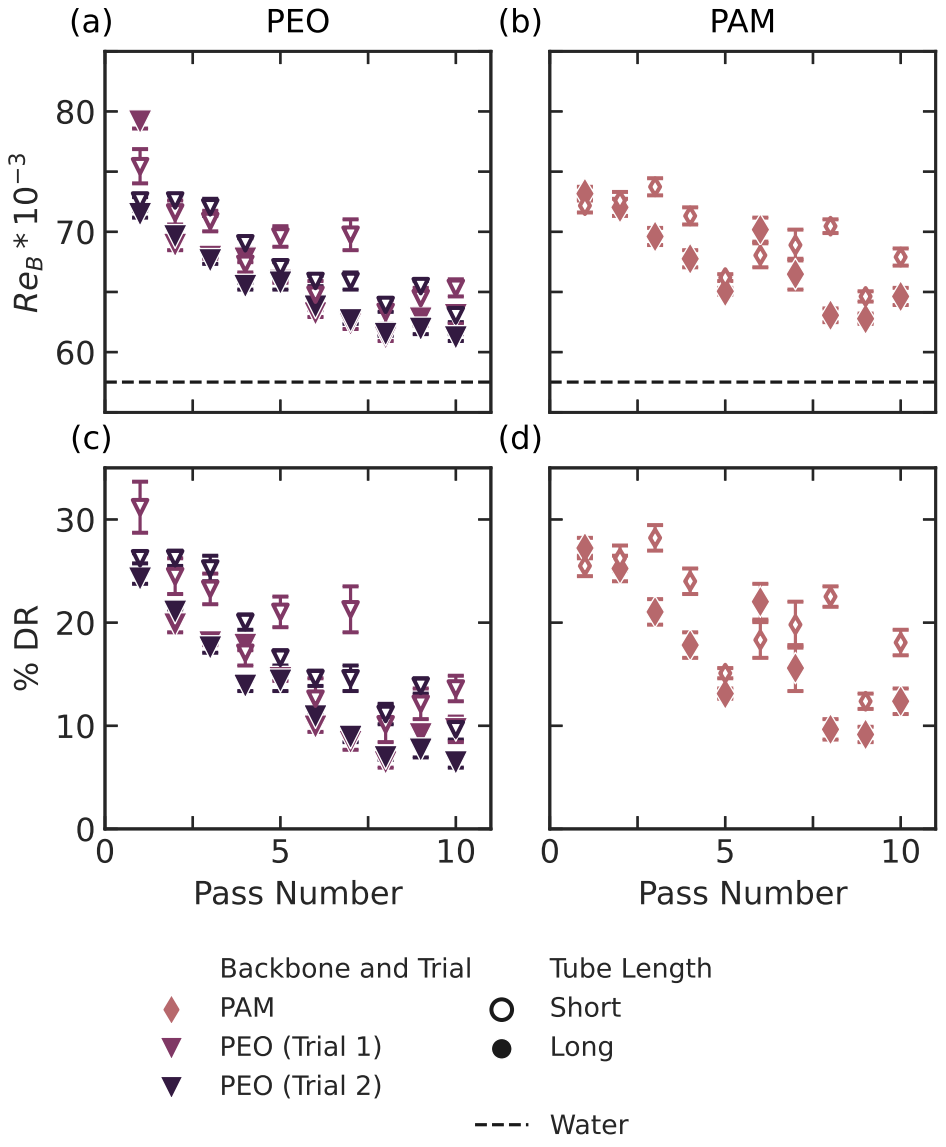

Figure 3.6: Changes with passes through the drag reduction instrument of sample solutions with as-prepared molecular weight and backbone of 6M PEO (two trials) and 6.7M PAM at as-prepared concentrations of 0.0066 wt %. (a) Bulk Reynolds number ($Re_B = 4\dot{m}/(\pi D\eta_{shear})$, where $\dot{m}$ is the mass flow rate, D is the tube diameter, and η_{shear} is the shear viscosity, approximately that of water) as a function of pass. Dashed line indicates the bulk Reynolds number for water in the short tube under the same conditions. (b) Calculated percent drag reduction as defined in Equation 3.1 as a function of pass. Vertical error bars represent 95% confidence intervals representing run-to-run variation in DoSER measurements (fitting errors are substantially smaller). Where error bars are not visible, the corresponding interval is within symbol size.

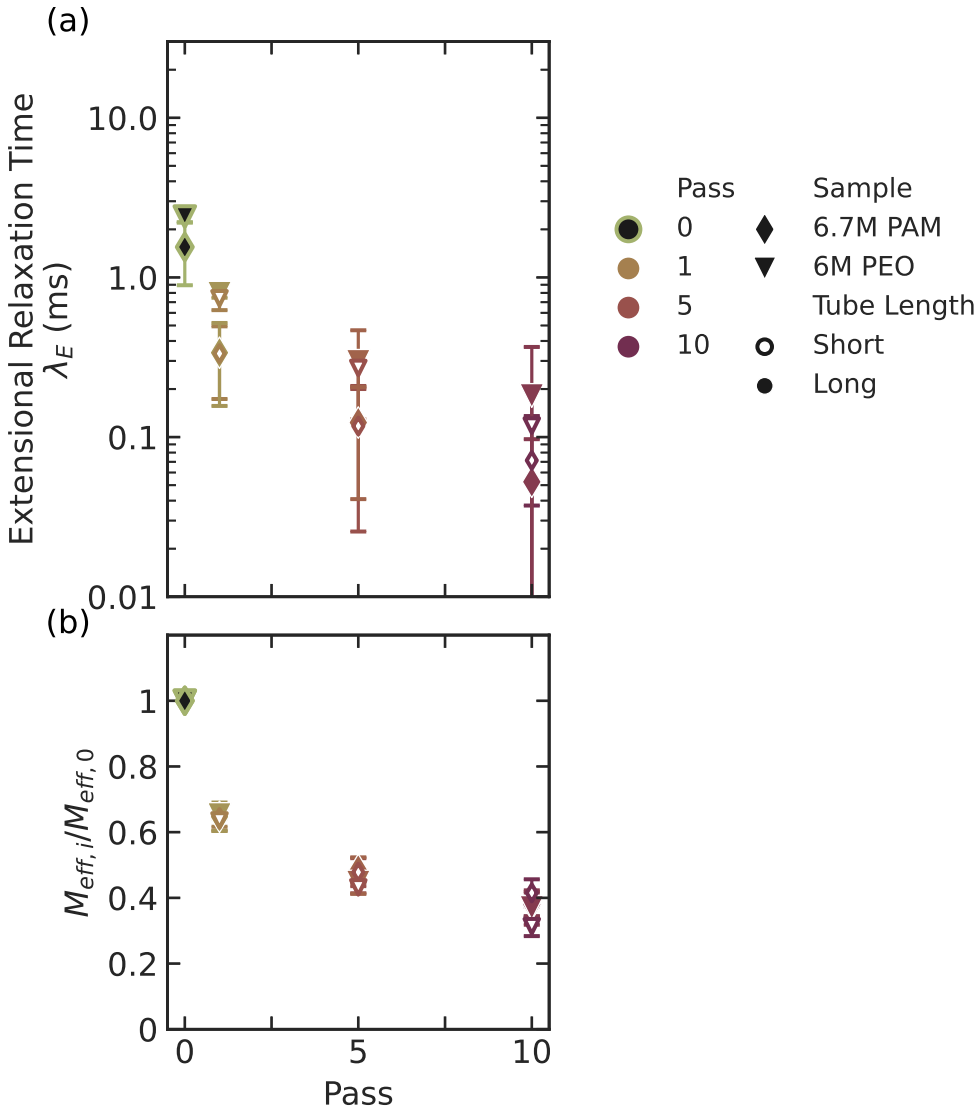

Figure 3.7: Changes with passes through the drag reduction instrument for solutions with as-prepared molecular weight and backbone of 6M PEO and 6.7M PAM at concentrations of 0.0066 wt %. (a) Extensional relaxation time (λ_E, ms) as a function of passes. (b) Ratio of effective molecular weight of degraded samples to initial effective molecular weight as a function of pass ($M_{eff,i}/M_{eff,0}$), given observed extensional relaxation time from (a) using Equation 2.3, assuming a constant total concentration of the solution. Vertical error bars represent 95% confidence intervals representing run-to-run variation in DoSER measurements (fitting errors are substantially smaller). Where error bars are not visible, the corresponding interval is within symbol size.

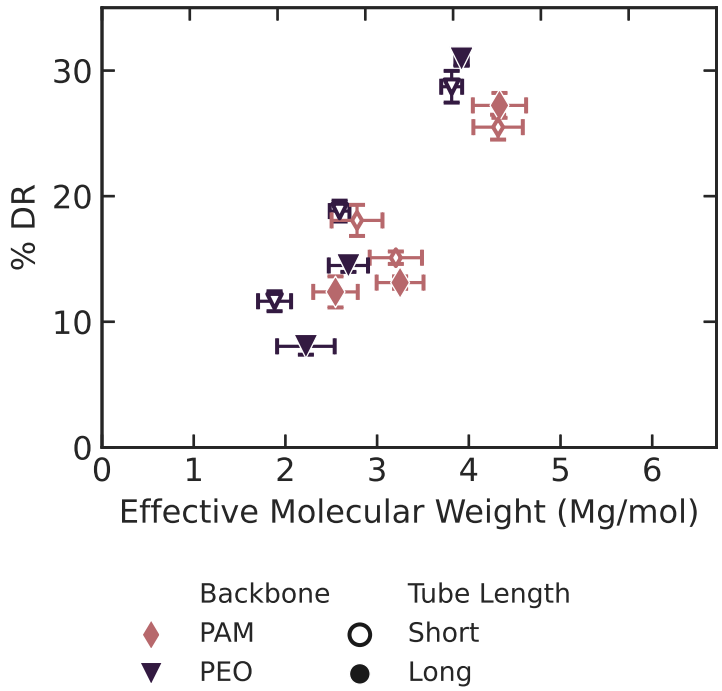

Figure 3.8: Percent drag reduction for solutions of 6M PEO (averaged over two trials) and 6.7M PAM after passes 1, 5, and 10 compared to water alone as a function of effective molecular weight (Mg/mol) calculated from extensional relaxation time measurements using Equation 2.3, assuming a constant total concentration of the solution. Vertical and horizontal error bars represent 95% confidence intervals on the respective measurements. Where error bars are not visible, the corresponding interval is within symbol size.

fluid. For safety reasons as well as equipment constraints, we were limited to 100 psi (0.69 MPa), 80 psi (0.55 MPa) with a safety margin. Because the instrument will eventually be used to test novel polymer additives, we were constrained to fluid volumes such that reasonable treat rates for polymeric drag reduction (50-100 ppm) will only require ∼1 g polymer per batch.

To enable optical access to observe pipe flow using PIV, we designed an optical section in quartz to meet the multiple needs of the experiments desired. For optical purposes, the viewing windows needs to be flat on at least two perpendicular sides: one for viewing with the camera, one for penetration of a laser

light sheet to create observable scattering of the fluorescent particles during PIV measurements. To establish a steady-state turbulent pipe flow, the tube must be sufficiently long and the inner wall must be circular throughout. For safety, the wall of the tube must be sufficiently thick to withstand pressures up to 100 psi (the upper end on the supply line and regulator). We met this set of constraints with the optical section depicted in Figure 3.3.

In addition to observations of the effects of polymeric drag reduction through PIV, we measure the mass flow of fluid through the instrument using a scale and use the steady-state rate of mass accumulation over time to determine the drag reduction relative to water alone. The tubing after the optical section and before the receiving tank can be exchanged to adjust the length and thus determine the pressure differential per length of tube (which is important to separate the effects of polymeric drag reduction from increased pressure loss in contraction and expansion due to polymers), which can be used to calculate the wall-shear-stress Reynolds number for comparison with PIV measurements. To keep the instrument tube lengths reasonable on a lab scale and with the pressure capabilities available, while still reaching the desired Reynolds numbers, our maximum total length is order 6 m.

For fair comparison of commericially available, traditional, long chain polymers with proposed end-associative polymers, we attempted to minimize potential degradation in the instrument. To avoid a known source of substantial degradation—pumping (see Chapter 2)—flow through the instrument occurs because of pressurization with air, rather than inducing additional highly extensional flow with a pump. To minimize contraction upon entering the tubing, a ball-valve was used as it permits the most open valve flow. Loading and pushback are both relatively gentle processes, the former done with only gravity-driven flow, the latter with relatively low air pressure. We still observe

substantial degradation of both poly(ethylene oxide) and polyacrylamide additives due to flow through the instrument, as discussed further below, but are able to ascribe it fully to the contraction-expansion flow.

Our instrument is able to reach bulk Reynolds numbers exceeding 50,000 for water at only 40 psi (0.28 MPa) (well below the upper limit of 80 psi), and we have observed drag reduction exceeding 30 % in preliminary polymeric drag reduction measurements, meeting our desired design criteria. Jacqueline Tawney is working towards full validation of the PIV measurements to establish canonical turbulent pipe flow and calibration of measurements close to the pipe wall to be able to observe polymer interactions with near-wall flow.

Localizing Degradation

Comparing the degradation for PEO at similar mass flow rates observed via decrease in extensional relaxation time of the solutions (and thus the effective molecular weight) in the contraction-expansion flow alone to the flow through the full drag reduction instrument indicates that the majority of degradation is happening in those elements, rather than in the pipe flow. The implication of these results is that during future particle image velocimetry (PIV) measurements, the portion of the flow observed in PIV will able to probe the polymer physics at a steady-state snapshot of degradation, rather than averaging over chains that are undergoing scission during turbulent flow in the optical section.

Degradation, however, does not appear to occur to a significant extent during loading or pushback of the fluid, isolating degradation observed to each full pressure pass. This information allows us to estimate the extension rates experienced in the contraction via the limiting extensional relaxation time after degradation ($\dot{\epsilon} \sim 1/\lambda_E$). At the flow rates for the drag reduction experiments, the extensional relaxation times reached by the PEO solutions in both the 15

psi contraction and drag reduction experiments were order 0.1 ms, implying that the contraction has extensional rates exceeding 10000 1/s.

Chain Scission and Drag Reduction

In agreement with the literature, we generally observed decreased drag reduction with degradation of the polymers in flow, with a relatively consistent decrease in mass flow rate with pass for the PEO solutions. The PAM solutions solutions, however, demonstrated an unusual increase in mass flow rate from pass 5 to 6 for both the short-tube and the long-tube experiments (Figure 3.6(b)). One potential cause could be the formation of polymer aggregates[7] in solution while the flow experiment was paused for sample collection after pass 5; however, a similar increase is not observed after pass 1 (where a sample was also collected), or in the PEO samples, which were more typically prone to aggregation in sample preparation. Another possible cause comes from the inherently coupled nature of the pipe flow and the contraction-expansion elements—because our pipe is lab-scale, not industrial scale, entrance and exit effects matter. In this instrument, drag reduction due to the polymers and the additional loss of pressure in the contraction and expansion steps due to the increased extensional viscosity are competing and the sum is observed via the mass flow rate. As degradation occurs, a tipping point may be reached where the PAM degrades enough to contribute less to the extensional flow in the contraction, yet still is an effective drag reducing agent, allowing for a net increase in the mass flow rate. Because of the limited amount of PAM available for this study, we were unable to repeat these results; further interrogation of whether this result is an artifact of our procedure or an indication of such a threshold is suggested for a future study. Both samples demonstrate decreasing extensional relaxation time with pass, and the percent of drag reduction appears

correlated (0.82) with the effective molecular weight calculated from those extensional relaxation times, even with two different reduced concentrations, as discussed below.

Comparing our two backbones, we might expect a priori that the 6M PEO would provide more drag reduction than the 6.7M PAM for two potential reasons. First, PEO has a longer effective length per unit mass than PAM due to the additional weight of PAM's side groups, leading to a higher extensibility.[14] Second, relatedly, PEO has a lower overlap concentration at equilibrium than PAM at similar molecular weights, indicating that at the a constant additive loading by mass chosen for comparison, PEO has a greater pervaded volume of solution when in its coil state. See Chapter 2 for a more extensive discussion of the differences between PEO and PAM in extensional flow and chain scission. Despite lower reduced concentration (c/c^* of 0.05 for PAM, 0.12 for PEO) and the shorter extended length (190,000 backbone atoms for PAM, 410,000 for PEO), PAM still demonstrated similar levels of drag reduction as a function of effective molecular weight of the backbone during degradation (Figure 3.8) and retained higher drag reduction after 10 passes of degradation. Additionally, in contrast to the results observed in chain scission in a pump (Chapter 2), we observed similar degradation in effective molecular weight for both PEO and PAM, where previously PAM degradation was less severe than that of PEO. The discrepancies in these results may point towards fundamentally different character of the flow in the pump used in Chapter 2 and through the contraction and expansion experienced here.

3.5 Conclusion

Through the combination of extensional rheology and bulk flow measurement, we were able to quantify both drag reduction and extensional relaxation times

of polymer solutions as they degraded, and monitor the relationship between the effective molecular weight and observed drag reduction relative to water.

Simultaneous particle image velocimetry and bulk flow measurements will allow for connection of the micro-scale effects of polymers on turbulent structures to the observed bulk drag reduction, and allow further evaluation of the theories developing on the mechanisms of turbulent drag reduction via simulations. Comparing the extensional properties of the solutions with their direct effects on drag reduction will inform better design of polymer additives and expansion of the design space of end-associative polymers tailored to maximize drag reduction and minimize permanent chain scission. Future studies have an opportunity to reveal at multiple length and energy scales the interactions of polymers and turbulence by partnering rheology and PIV with the theoretical framework of resolvent analysis.

References

[1] M. D. Graham. "Drag Reduction and the Dynamics of Turbulence in Simple and Complex Fluids". In: *Physics of Fluids* 26.10 (Oct. 2014), p. 101301. ISSN: 1070-6631, 1089-7666. DOI: 10.1063/1.4895780. URL: http://scitation.aip.org/content/aip/journal/pof2/26/10/10.1063/1.4895780 (visited on 03/17/2016).

[2] S. U. Choi, Y. I. Cho, and K. E. Kasza. "Degradation Effects of Dilute Polymer Solutions on Turbulent Friction and Heat Transfer Behavior". In: *Journal of Non-Newtonian Fluid Mechanics* 41.3 (Feb. 1992), pp. 289–307. ISSN: 03770257. DOI: 10.1016/0377-0257(92)87003-T. URL: https://linkinghub.elsevier.com/retrieve/pii/037702579287003T (visited on 11/19/2020).

[3] T. Moussa and C. Tiu. "Factors Affecting Polymer Degradation in Turbulent Pipe-Flow". In: *Chemical Engineering Science* 49.10 (May 1994), pp. 1681–1692. ISSN: 0009-2509. DOI: 10.1016/0009-2509(93)E0029-C.

[4] J. M. J. Den Toonder et al. "Degradation Effects of Dilute Polymer Solutions on Turbulent Drag Reduction in Pipe Flows". In: *Applied scientific research* 55.1 (1995), pp. 63–82. URL: http://link.springer.com/article/10.1007/BF00854224 (visited on 05/05/2016).

[5] V. N. Kalashnikov. "Degradation Accompanying Turbulent Drag Reduction by Polymer Additives". In: (2002), p. 18.

[6] M. W. Liberatore et al. "Turbulent Drag Reduction of Polyacrylamide Solutions: Effect of Degradation on Molecular Weight Distribution". In: (2004), p. 10.

[7] E. J. Soares. "Review of Mechanical Degradation and De-Aggregation of Drag Reducing Polymers in Turbulent Flows". In: *Journal of Non-Newtonian Fluid Mechanics* 276 (Feb. 2020), p. 104225. ISSN: 03770257. DOI: 10.1016/j.jnnfm.2019.104225. URL: https://linkinghub.elsevier.com/retrieve/pii/S0377025719304197 (visited on 11/19/2020).

[8] M.-H. Wei et al. "Megasupramolecules for Safer, Cleaner Fuel by End Association of Long Telechelic Polymers". In: *Science* 350.6256 (Oct. 2, 2015), pp. 72–75. ISSN: 0036-8075, 1095-9203. DOI: 10.1126/science.aab0642. URL: http://www.sciencemag.org/cgi/doi/10.1126/science.aab0642 (visited on 03/17/2016).

[9] M. D. Graham. "Drag Reduction in Turbulent Flow of Polymer Solutions". In: *Rheology Reviews* 2 (2004), pp. 143–170.

[10] "Some Distinctive Rheological Concepts and Phenomena". In: *Rheology Series*. Ed. by R. Tanner and K. Walters. Vol. 7. Elsevier, 1998, pp. 159–186. ISBN: 978-0-444-82945-0. DOI: 10.1016/S0169-3107(98)

80008-7. URL: https://linkinghub.elsevier.com/retrieve/pii/S0169310798800087 (visited on 04/28/2022).

[11] B. A. Toms. "Some Observations on the Flow of Linear Polymer Solutions through Straight Tubes at Large Reynolds Numbers". In: *Proceedings of the International Congress on Rheology* II (1949), pp. 135–141.

[12] B. A. Toms. "On the Early Experiments on Drag Reduction by Polymers". In: *Physics of Fluids* 20.10 (1977), S3. ISSN: 00319171. DOI: 10.1063/1.861757. URL: http://scitation.aip.org/content/aip/journal/pof1/20/10/10.1063/1.861757 (visited on 03/18/2016).

[13] C. M. White and M. G. Mungal. "Mechanics and Prediction of Turbulent Drag Reduction with Polymer Additives". In: *Annual Review of Fluid Mechanics* 40.1 (Jan. 2008), pp. 235–256. ISSN: 0066-4189, 1545-4479. DOI: 10.1146/annurev.fluid.40.111406.102156. URL: http://www.annualreviews.org/doi/abs/10.1146/annurev.fluid.40.111406.102156 (visited on 12/10/2015).

[14] L. Xi. "Turbulent Drag Reduction by Polymer Additives: Fundamentals and Recent Advances". In: *Physics of Fluids* 31.12 (Dec. 1, 2019), p. 121302. ISSN: 1070-6631, 1089-7666. DOI: 10.1063/1.5129619. URL: http://aip.scitation.org/doi/10.1063/1.5129619 (visited on 07/13/2021).

[15] P. Virk. "The Toms Phenomenon - Turbulent Pipe Flow of Dilute Polymer Solutions". Cambridge, MA: Massachusetts Institute of Technology, Nov. 1966. 454 pp. URL: https://dspace.mit.edu/bitstream/handle/1721.1/15484/11163935-MIT.pdf?sequence=2 (visited on 07/07/2016).

[16] P. S. Virk et al. "The Toms Phenomenon: Turbulent Pipe Flow of Dilute Polymer Solutions". In: *Journal of Fluid Mechanics* 30.02 (1967), pp. 305–328. URL: http://journals.cambridge.org/abstract_S0022112067001442 (visited on 03/17/2016).

[17] P. S. Virk, H. S. Mickley, and K. A. Smith. "The Ultimate Asymptote and Mean Flow Structure in Toms' Phenomenon". In: *Journal of Applied Mechanics* 37.2 (1970), p. 488. ISSN: 00218936. DOI: 10.1115/1.3408532. URL: http://AppliedMechanics.asmedigitalcollection.asme.org/article.aspx?articleid=1399383 (visited on 08/18/2016).

[18] P. S. Virk. "Drag Reduction Fundamentals". In: *AIChE Journal* 21.4 (July 1975), pp. 625–656.

[19] C. M. White, Y. Dubief, and J. Klewicki. "Re-Examining the Logarithmic Dependence of the Mean Velocity Distribution in Polymer Drag Reduced Wall-Bounded Flow". In: *Physics of Fluids* 24.2 (Feb. 2012), p. 021701. ISSN: 1070-6631, 1089-7666. DOI: 10.1063/1.3681862. URL:

http://aip.scitation.org/doi/10.1063/1.3681862 (visited on 09/27/2019).

[20] J. M. Lopez, G. H. Choueiri, and B. Hof. "Dynamics of Viscoelastic Pipe Flow at Low Reynolds Numbers in the Maximum Drag Reduction Limit". In: *Journal of Fluid Mechanics* 874 (Sept. 10, 2019), pp. 699–719. ISSN: 0022-1120, 1469-7645. DOI: 10.1017/jfm.2019.486. URL: https://www.cambridge.org/core/product/identifier/S0022112019004865/type/journal_article (visited on 06/16/2020).

[21] M. D. Warholic, G. M. Schmidt, and T. J. Hanratty. "The Influence of a Drag-Reducing Surfactant on a Turbulent Velocity Field". In: *Journal of Fluid Mechanics* 388 (June 1999), pp. 1–20. ISSN: 1469-7645, 0022-1120. DOI: 10.1017/S0022112099004498. URL: https://www.cambridge.org/core/journals/journal-of-fluid-mechanics/article/abs/influence-of-a-dragreducing-surfactant-on-a-turbulent-velocity-field/61C146D81503049603D3C6A050C84F98 (visited on 04/28/2022).

[22] M. D. Warholic et al. "A Study with Particle-Image Velocimetry of the Influence of Drag-Reducing Polymers on the Structure of Turbulence". In: *Experiments in Fluids* 31.5 (Nov. 1, 2001), pp. 474–483. ISSN: 0723-4864, 1432-1114. DOI: 10.1007/s003480100288. URL: http://link.springer.com/10.1007/s003480100288 (visited on 04/29/2022).

[23] C. M. White, V. S. R. Somandepalli, and M. G. Mungal. "The Turbulence Structure of Drag-Reduced Boundary Layer Flow". In: *Experiments in Fluids* 36.1 (Jan. 1, 2004), pp. 62–69. ISSN: 0723-4864, 1432-1114. DOI: 10.1007/s00348-003-0630-0. URL: http://link.springer.com/10.1007/s00348-003-0630-0 (visited on 04/29/2022).

[24] D. Samanta et al. "Elasto-Inertial Turbulence". In: *Proceedings of the National Academy of Sciences* 110.26 (June 25, 2013), pp. 10557–10562. ISSN: 0027-8424, 1091-6490. DOI: 10.1073/pnas.1219666110. URL: http://www.pnas.org/cgi/doi/10.1073/pnas.1219666110 (visited on 08/26/2016).

[25] L. Xi and M. D. Graham. "Dynamics on the Laminar-Turbulent Boundary and the Origin of the Maximum Drag Reduction Asymptote". In: *Physical Review Letters* 108.2 (2012). DOI: 10.1103/PhysRevLett.108.028301. URL: http://link.aps.org/doi/10.1103/PhysRevLett.108.028301.

[26] G. H. Choueiri, J. M. Lopez, and B. Hof. "Exceeding the Asymptotic Limit of Polymer Drag Reduction". In: *Physical Review Letters* 120.12 (Mar. 19, 2018). ISSN: 0031-9007, 1079-7114. DOI: 10.1103/PhysRevLett.120.124501. URL: https://link.aps.org/doi/10.1103/PhysRevLett.120.124501 (visited on 05/17/2019).

[27] B. J. McKeon and A. S. Sharma. "A Critical-Layer Framework for Turbulent Pipe Flow". In: *Journal of Fluid Mechanics* 658 (Sept. 2010), pp. 336–382. ISSN: 0022-1120, 1469-7645. DOI: 10.1017/S002211201000176X. URL: http://www.journals.cambridge.org/abstract_S002211201000176X (visited on 03/17/2016).

[28] B. J. McKeon, A. S. Sharma, and I. Jacobi. "Experimental Manipulation of Wall Turbulence: A Systems Approacha)". In: *Physics of Fluids (1994-present)* 25.3 (2013), p. 031301. URL: http://scitation.aip.org/content/aip/journal/pof2/25/3/10.1063/1.4793444 (visited on 08/09/2016).

[29] R. Learsch. "Investigation in Experimental Conditions and Automation of Dripping-onto-Substrate Rheology". American Chemical Society Spring Meeting (San Diego, CA). Mar. 23, 2022.